

To appear in *Astrophysical Journal*, Dec 20 issue

N-BODY SIMULATIONS OF COMPACT YOUNG CLUSTERS NEAR THE GALACTIC CENTER

Sungsoo S. Kim¹, Donald F. Figer², Hyung Mok Lee³, and Mark Morris¹

ABSTRACT

We investigate the dynamical evolution of compact young star clusters (CYCs) near the Galactic center (GC) using Aarseth's Nbody6 codes. The relatively small number of stars in the cluster (5,000–20,000) makes real-number N-body simulations for these clusters feasible on current workstations. Using Fokker-Planck (F-P) models, Kim, Morris, & Lee (1999) have made a survey of cluster lifetimes for various initial conditions, and have found that clusters with a mass $\lesssim 2 \times 10^4 M_\odot$ evaporate in ~ 10 Myr. These results were, however, to be confirmed by N-body simulations because some extreme cluster conditions, such as strong tidal forces and a large stellar mass range participating in the dynamical evolution, might violate assumptions made in F-P models. Here we find that, in most cases, the CYC lifetimes of previous F-P calculations are 5–30 % shorter than those from the present N-body simulations. The comparison of projected number density profiles and stellar mass functions between N-body simulations and *HST*/NICMOS observations by Figer et al. (1999) suggests that the current tidal radius of the Arches cluster is ~ 1.0 pc, and the following parameters for the initial conditions of that cluster: total mass of $2 \times 10^4 M_\odot$ and mass function slope for intermediate-to-massive stars of 1.75 (the Salpeter function has 2.35). We also find that the lower stellar mass limit, the presence of primordial binaries, the amount of initial mass segregation, and the choice of initial density profile (King or Plummer models) do not significantly affect the dynamical evolution of CYCs.

Subject headings: celestial mechanics, stellar dynamics — Galaxy: center — methods: n-body simulations — galaxies: star clusters

¹Division of Astronomy, University of California, Los Angeles, CA, 90095-1562; sskim@astro.ucla.edu; morris@astro.ucla.edu

²Space Telescope Science Institute, 3700 San Martin Drive, Baltimore, MD 21218; figer@stsci.edu

³Astronomy Program, SEES, Seoul National University, Seoul 151-742, Korea; hmlee@astro.snu.ac.kr

1. INTRODUCTION

The Arches (G0.121+0.017) and Quintuplet (AFGL 2004) clusters are two extraordinary star clusters near the Galactic center. They are very young (< 5 Myr), compact ($\lesssim 1$ pc), and only 20–30 parsecs away from the Galactic center (GC) in projection, while they appear to be as massive as the smallest Galactic globular clusters ($\sim 10^4 M_\odot$; Figer et al. 1999). These compact young clusters (CYCs) have several interesting dynamical characteristics that distinguish them from globular clusters: 1) CYCs have very short dynamical and half-mass relaxation timescales ($t_{dyn} \sim 10^{5-6}$ yr and $t_{rh} \sim 10^{6-7}$ yr, respectively); 2) CYCs are situated in strong tidal fields (the tidal radius of a $10^4 M_\odot$ cluster located 30 pc from the Galactic center is ~ 1 pc); and 3) mass segregation may occur on a timescale shorter than the lifetimes of the most massive stars, such that those massive stars play an important role in the dynamical evolution of the cluster (for more details on timescales and the effects of tidal fields, see Kim, Morris, & Lee, 1999; hereafter KML).

The fact that we currently observe only two such young clusters near the GC (in addition to the central cluster right at the GC) raises a natural question about the lifetimes of CYCs. Using anisotropic Fokker-Planck (F-P) models, KML surveyed lifetimes of CYCs for various initial mass functions (IMFs), cluster masses (M), and Galactocentric radii (R_g), and found that clusters with $M \lesssim 2 \times 10^4 M_\odot$ and $R_g \lesssim 100$ pc evaporate in $\lesssim 10$ Myr.⁴ These unparalleled, short evaporation times (t_{ev} ; defined here as the time by which M , the cluster mass inside the tidal radius, becomes 5 % of its initial value) of CYCs are first due to short t_{dyn} and t_{rh} , and strong tidal forces, but the mass loss accompanying the evolution of massive stars is also responsible for shortening t_{ev} of clusters that last longer than ~ 3 Myr.

F-P models are statistical models involving distribution functions. It is the statistical stability and fast computing time of the F-P models that the survey-type study by KML required. Takahashi & Portegies Zwart (1998) found good agreement between anisotropic F-P models and N-body simulations for globular clusters by adopting an “apocenter criterion” and an appropriate coefficient for the speed of star removal beyond the tidal radius (KML adopted these as well). However, some extreme conditions of CYCs may be inconsistent with the assumptions inherent to F-P models. As discussed in KML, the conditions required by F-P models, $t_{dyn} \ll t_{rh}$ and $t_{dyn} \ll t_{se}$ (t_{se} is the stellar evolution timescale) may be violated, especially in the core at certain epochs. Moreover, the active participation of a large mass range of stars in the dynamics, which is another peculiarity of CYCs, is difficult to realize in F-P models that embody a mass spectrum with a restricted number (usually 10–20) of discrete mass components. A greater number of components would better express the mass spectrum, but then the computation time would

⁴Portegies Zwart et al. (1999) have studied with N-body models the evolution of R136, a compact, young star cluster in the 30 Doradus region of the Large Magellanic Cloud. This cluster resembles the CYCs near the GC in many ways, except for the tidal forces, which are speculated to be much weaker than those for the CYCs near the GC. We note that Portegies Zwart et al. (2000) are independently working on N-body simulations targeted for the CYCs near the GC at the moment of the submission of the present paper.

become accordingly longer. On the other hand, too small a number of components would not properly realize the whole mass spectrum. By fixing the number of stars in the most massive components, KML tried to carefully account for a relatively small number of the most massive stars. Yet, the results from such a treatment are to be confirmed by more realistic models, N-body simulations.

CYCs, estimated to have $\sim 10^{3-4}$ stars, are one of a few classes of systems for which real-number N-body simulations are feasible on current workstations. Among many virtues of N-body simulations, the natural realization of the mass spectrum and the tidal fields is particularly beneficial to the study of CYCs. These benefits allow N-body simulations to treat mass segregation and evaporation of stars exactly, thus providing better density profiles and mass spectra as a function of radius. These are photometric observables, and are partially available from the *HST*/NICMOS observations of the Arches and Quintuplet (Figer et al. 1999; the partial availability is owed to crowding at the cluster center and to the detection limit at the faint end of the luminosity function). The Arches and Quintuplet are estimated to be only ~ 2 and ~ 4 Myr old, respectively (Figer et al. 1999), but their currently observed structures must already have deviated from the initial ones due to their rapid dynamical evolution. With both real-number N-body simulations and HST observations of the two clusters in hand, one has a rare chance of deriving not only the current characteristics of these systems, but their initial conditions as well.

In the present study, we perform a series of N-body simulations 1) to compare the lifetimes of CYCs with those from F-P models obtained by KML, 2) to find the initial cluster conditions that best match the current observations of CYCs, and 3) to test the effects of initial mass segregation and different initial density profiles on the dynamical evolution of the CYCs.

2. SIMULATION MODELS

For N-body simulations in the present study, we use the most recent version of Aarseth's N-body codes, Nbody6 (Aarseth 1999 and references therein). We modified the Nbody6 codes to implement the full, non-truncated tidal forces, and we adopted the prescription for stellar evolution used in KML for consistency (see KML for details on the stellar evolution). The upper stellar mass limit, m_u , is $150 M_\odot$, and the lower mass limit, m_l , is $0.1 M_\odot$ or $1 M_\odot$. We set the cluster to initially fill the tidal radius, and remove stars outside 5 times the tidal radius.

For initial conditions of the cluster and the Galactic tidal field, we also follow prescriptions of KML: We adopt single-mass King models (with a King parameter $W_0 = 4$) and single power-law mass functions; The Galactic mass M_g inside a Galactocentric radius R_g is given by

$$M_g = 2 \times 10^8 M_\odot \left(\frac{R_g}{30 \text{ pc}} \right)^{1.2} \quad (1)$$

(from Genzel & Townes, 1987). Then the tidal radius of the cluster, R_t , becomes

$$\begin{aligned} R_t &= \left(\frac{M}{2M_g} \right)^{1/3} R_g \\ &\simeq 5.3 \times 10^{-3} \text{ pc} \left(\frac{M}{M_\odot} \right)^{1/3} \left(\frac{R_g}{\text{pc}} \right)^{0.6}. \end{aligned} \quad (2)$$

The equations of motions are integrated in the rotating frame, and tidal forces are calculated from the Galactic potential corresponding to equation (1).

3. N-BODY VS. FOKKER-PLANCK

In order to compare t_{ev} of N-body and F-P calculations, we performed N-body simulations of several representative models in KML that have number of stars, N , smaller than $\sim 15,000$. This criterion excludes $m_l = 0.1 M_\odot$ models with the exponent of the power-law IMF, α (defined as in $dN \propto m^{-\alpha} dm$), larger than or equal to 2.

The lifetimes of 9 N-body simulations performed in the present study are shown in Table 1 along with those from F-P calculations of KML.⁵ This set of 9 models represent different M (models 1 & 5), different α (models 1, 8, 13, & 23), different m_l (models 3 & 8; models 13 & 15), and different R_g (models 13, 43, & 44). We find that N-body calculations always give longer t_{ev} than F-P calculations, and that the fractional difference of t_{ev} between two calculations, $\Delta't_{ev}$ ($\equiv [N\text{body-FP}]/N\text{body}$), does not show any particular correlation with N . The biggest $\Delta't_{ev}$, 59 %, is for model 43, for which the IMF is quite flat ($\alpha = 1.75$) and the cluster evaporates before significant stellar evolution starts. This implies that $\Delta't_{ev}$ is larger for smaller α (compare to model 5, which has as short t_{ev} as model 43 but $\Delta't_{ev}$ of only 8 %), but that the stellar evolution has the effect of diminishing $\Delta't_{ev}$ (cf. model 44, which also has $\alpha = 1.75$ but $\Delta't_{ev}$ of only 16 %). We performed the N-body and F-P calculations for model 13 without stellar evolution, and find that the new t_{ev} 's are 4.5 and 2.5 Myr, respectively (model 13 is our baseline model because we later find that it best matches the observations; see § 4). This indicates that the speed of the pure (i.e., no stellar evolution) dynamical evolution of F-P models by KML is considerably overestimated.

We attribute shorter t_{ev} 's of F-P calculations to the underestimated choice of N_u (the number of stars in the most massive bin; the same as N_{15} when the number of mass bins, N_{bin} , is 15 as in KML) by KML. The mass bins of F-P models by KML were chosen to make N_u constant, so that the significance of the most massive bins of models with different IMFs would be the same.

⁵The lifetimes from N-body simulations are subject to the statistical fluctuation which may be significant for models with N smaller than a few thousands. We find that our models have fluctuations from one run to the next mostly smaller than 10 %. Such relatively small fluctuations are due to our definition of t_{ev} (see § 1), which avoids the late phase of the evolution that suffers most from statistical fluctuations.

The larger N_u , the smaller the characteristic mass of the most massive bin, thus the smaller the effective mass range (the lower and upper mass limits are not a function of N_u). Since a larger effective mass range gives faster mass segregation and thus faster ejection of lighter stars, a smaller N_u results in smaller t_{ev} . For N_{bin} cannot be infinitely large for a practical reason, F-P models have difficulties with dealing with a very large mass range, and F-P results may depend on the way of binning the mass with a limited number of components (bins). The choice of $N_u = 50$ in KML was arbitrary, and one may tune the F-P t_{ev} values to N-body t_{ev} values by controlling this parameter. We find that a new F-P calculation for model 13 with no stellar evolution and $N_u = 250 - 300$ gives a t_{ev} value that matches the N-body results without stellar evolution, 4.5 Myr. In conclusion, the choice of $N_u = 50$ in KML was too small, thus KML underestimated t_{ev} , but such underestimation was not significant for most cases because the amount of mass loss from stellar evolution after ~ 2 Myr accelerates the evaporation of clusters.

Figure 1 compares the volume density profiles of N-body and F-P calculations for model 13 at 1 and 2 Myr. For this F-P calculations, $N_u = 250$ and $N_{\text{bin}} = 10$ (instead of 15 as in KML) were used. For $N_u = 250$, N_{bin} larger than 10 would give negative β values (see KML for definition of β ; a negative β gives smaller numbers of stars for lighter mass bins). At $t = 1$ Myr, the two density profiles differ only near and outside R_t (the small deviation at the core is probably due to small number statistics), but the F-P calculation significantly underestimates the density outside R_t . At $t = 2$ Myr, the deviation starts at smaller radii, and the power-law slope of the F-P density profile is steeper than the N-body slope by 0.3 to 0.4 inside R_t . Such a difference makes the cluster mass inside the tidal radius of the F-P calculation always somewhat smaller than that of the N-body calculation. Figure 2 compares the evolution of cluster mass inside the tidal radius, M , of N-body and F-P calculations for model 13. Stellar evolution was not included in these calculations in order to see the effect of tidal fields only, and $N_u = 250$ and $N_{\text{bin}} = 10$ were used for the F-P calculation. The figure shows that the mass loss rate from the cluster differs especially during the early phase of evolution. We also find that the α value of the F-P calculation decreases faster with time, having 0.1 to 0.3 smaller (shallow mass function) values, than those of the N-body simulation at most times. N-body models are more realistic than F-P models, whose observables are here found to have non-negligible discrepancies from N-body models; therefore for comparison with the observed structures of the CYCs, N-body simulations should be preferred over F-P models.

4. INITIAL CONDITIONS OF THE ARCHES

4.1. Comparison with Observations

In spite of the very young ages of the CYCs, the observed properties of CYCs should differ from their initial status because of the cluster’s rapid dynamical evolution. Thus one should compare numerical simulations of cluster evolution with observations to infer the initial conditions of the cluster. As discussed in § 3, N-body simulations provide the most accurate information

on the dependence of the stellar distribution on stellar mass. In this section, we use our N-body simulations to find initial conditions of the Arches cluster from comparisons with *HST*/NICMOS photometric observations by Figer et al. (1999). The Quintuplet cluster has a largely dispersed distribution (probably because it is in the final disruption phase), so dynamical information from its image is very limited.

Dynamical information from the photometric image of a cluster can be found from the surface density profiles and the mass distribution functions as a function of radius. When the photometry is complete down to the faintest stars, the overall stellar mass function, total cluster mass, and degree of mass segregation are obtained from the above two observables. However, the *HST* observations of the Arches were limited by crowding in the core and by the background confusion in the outer regions. Using the mass-K magnitude relation of Meynet et al. (1994) and adopting an extinction at K band of 3.1, Figer et al. (1999) estimate that their *HST* Arches photometry is complete down to $m \simeq 20 M_{\odot}$ for $r > 3''$, or 0.12 pc, and to $m \simeq 8 M_{\odot}$ for $r > 5.''25$, or 0.2 pc (the distance to the GC is assumed to be 8 kpc in the present study), and that the background confusion limit lies between 3 and $5 M_{\odot}$. For this reason, we only use stars having $m > 20 M_{\odot}$ ($F205W < 15$ mag, where $F205W$ is the underreddened, apparent Vega magnitude of the NICMOS F205W filter) for the surface number density profile, and $m > 8 M_{\odot}$ ($F205W < 17$ mag) for estimating the mass spectrum. The number of stars heavier than $8 M_{\odot}$ outside its crowding limit, 0.2 pc, is 232, which is not enough to give reliable information on the mass spectrum as a function of radius. Therefore we adopt the simplest way of measuring the mass function and the mass segregation: we count the number of stars in two mass bins ($8 \leq m/M_{\odot} < 20$ and $20 \leq m/M_{\odot}$), each in two radius bins ($0.2 \leq r/\text{pc} < 0.4$ and $0.4 \leq r/\text{pc} < 0.8$). In principle, one can find the initial conditions (or several sets of initial conditions) of a cluster by comparing these number counts and the density profiles of numerical simulations and observations.

We start with IMFs that give the observed number of massive stars, which, for the Arches cluster, is expected to be very close to its initial value (the estimated age of the Arches, ~ 2 Myr, is before significant stellar evolution). The observations require the IMF to have $N(> 30 M_{\odot})$ of 150 ($30 M_{\odot}$ stars are complete down to $r \simeq 0.06$ pc). The surface number density profiles for $M \geq 20 M_{\odot}$ (Σ_{20}) at 1 or 2 Myr, and the number count evolutions of N-body simulations of models 13, 21, and 22 are plotted in Figures 3 and 4 along with observations (the count numbers from observations are given in Table 2). These three models have $N(> 30 M_{\odot})$ values of about 150 but different α values (see Table 3). Σ_{20} plots in Figure 3 show that all three models agree well with the observation, which implies that our choice of the bulge mean density at the location of the cluster is appropriate because the mean bulge density determines the tidal radius of the cluster (this does not necessarily prove that our choices of the bulge mass profile, eq. [1], and R_g for these models, 30 pc, are correct since the bulge mean density is a combination of two parameters; see below). The R_t values of our N-body models shown in Figure 3 are 1.0–1.2 pc. Figure 4 shows that the observed number counts best agree with model 13 ($\alpha = 1.75$) at time $t = 1$ –2 Myr. Model 21 ($\alpha = 1.5$) gives slightly smaller counts than observations, but considering the uncertainty in the

mass-magnitude relation, we cannot exclude the possibility that model 21 is applicable. On the other hand, model 22 ($\alpha = 2$) significantly over-predicts the number of stars in lighter mass bins, except at $t \gtrsim 3$ Myr, by which time the cluster would be in a disruption phase. We conclude that the best α value suggested by these comparisons to observations is 1.75.

This finding may be, in fact, limited to the high mass regime only, where the comparison is actually made. However, for the above best-fit mass function, the stars with $m \geq 8 M_{\odot}$ already constitute more than 70 % of the total mass, thus the above α value may be considered representative.

The projected distance from the GC to the Arches is ~ 20 pc, but the true distance is unknown. Furthermore, the bulge mass distribution at a few tens of parsecs from the GC is uncertain. While the infrared light distribution observed by Becklin & Neugebauer (1968) implies a density profile $\propto R_g^{-1.8}$ (eq. [1] exhibits this profile), the radial velocity observations in radio frequencies for the same region suggest a shallower density drop ($\propto R_g^{-1.5}$) between 30 and 100 pc, leading to a steeper enclosed-mass increase:

$$M_g \simeq 8 \times 10^7 M_{\odot} \left(\frac{R_g}{30 \text{ pc}} \right)^{1.5} \quad (3)$$

(Lindqvist, Habing, & Winnberg 1992). The tidal environment of the cluster is mostly determined by the mean density, M_g/R_g^3 . We performed the best-fit model found above ($\alpha = 1.75$; model 13) with different tidal environments: models located at $R_g = 20$ pc (model 19) and 50 pc (model 14) with our standard bulge mass distribution, equation (1). The latter is equivalent to the case of $R_g = 30$ pc with a bulge mass distribution of equation (3). We find that Σ_{20} of models 13, 14, and 19 can be all nicely fit to the observed Σ_{20} at $t = 1\text{--}2$ Myr, and that the number counts of models 14 and 19 showed worse agreement to observations than model 13, but the agreement was still at the acceptable level. We conclude that our comparisons do not rule out the possibility of $R_g = 20$ pc and 50 pc, but favor the $R_g = 30$ pc case.

Model 15 has the same initial conditions as our best-fit model, model 13, except $m_l = 0.1 M_{\odot}$ instead of $1 M_{\odot}$. We find that t_{ev} of model 15 is only $\sim 10\%$ longer than that of model 13 (see Table 3). This confirms the finding by KML that t_{ev} does not sensitively depend on m_l when $\alpha \lesssim 2$. This phenomenon is caused by two factors: 1) for a model with $\alpha = 1.75$ and $m_u = 150 M_{\odot}$, the mass between $0.1 M_{\odot}$ and $1 M_{\odot}$ constitutes only 15 % of the total mass, and 2) the lightest stars are rapidly ejected from the cluster during the early phases due to the large m_u/m_l ratio. However, the number counts of model 15 agree well with observations only after $t = 2.4$ Myr, by which time the Arches cluster would be in the disruption phase and would have a structure as dispersed as the Quintuplet. Thus the observations more support our model with $m_l = 1 M_{\odot}$ than $0.1 M_{\odot}$.

One of the most commonly used IMFs for the Galactic disk, the Scalo mass function (Scalo 1986), has $\alpha = 2.7$ for $m \geq 1 M_{\odot}$, implying that the best-fit α value obtained here for the Arches cluster is considerably flatter than that for the disk. This fact, together with $m_l = 1 M_{\odot}$

being favored over $m_l = 0.1 M_\odot$, appears to support the arguments by Morris (1993) that the non-standard star formation environment near the GC may lead to an IMF skewed toward relatively massive stars and having an elevated lower mass cutoff.

4.2. Primordial Binaries

So far, we have not considered primordial binaries. Camera 2 of the *HST*/NICMOS instrument (used by Figer et al. 1999) has an angular resolution of about 1 pixel size of the detector (0.075''), which is ~ 600 AU at the distance of the GC. Thus binary systems with a semi-major axis smaller than few hundred AU are not resolved, and the presence of a significant number of primordial binaries in the cluster may affect our number count analysis above by decreasing number counts and/or by moving a primary star to a more massive mass bin (the number of dynamical binaries, i.e., binaries formed through close encounters, at a given moment is only a few, if any, for the whole cluster lifetime). To see the effects of primordial binaries on the number counts, we performed two simulations of model 13 with primordial binary fractions, f_{bin} , of 25 % and 50 %. The fraction is defined as

$$f_{bin} \equiv \frac{N_{bin}}{N_{bin} + N_{sing}}, \quad (4)$$

where N_{bin} and N_{sing} are the numbers of binary systems and single stars, respectively. Thus the percentages of stars in binary systems for $f_{bin} = 25$ % and 50 % are 40 % and 67 %, respectively. These relatively ‘moderate’ f_{bin} values, compared to > 50 % used in N-body simulations for open clusters (Kroupa, Petr, & McCaughrean 1999, for example) may be justified by an argument by Durisen & Sterzik (1994) that binary formation from fragmentation of collapsing and rotating clouds or from a gravitational instability of massive protostellar disks is more likely in low-temperature clouds (the central molecular zone in the inner few hundred pc of the Galactic bulge has significantly elevated temperatures, ~ 70 K). The initial companion-mass-ratio distribution is obtained by random pairing of stars, and the initial eccentricity distribution is assumed to be thermally relaxed. For the initial period distribution, we adopt equation (8) of Kroupa (1995a), which approximates the distribution of binary systems in the Galactic disk. This initial distribution is evolved prior to the start of the N-body integration to account for the “pre-main-sequence eigenevolution” (the evolution in orbital parameters due to internal processes such as tidal circularization during the pre-main-sequence; see Kroupa 1995a for details).

We find that the t_{ev} values of $f_{bin} = 25$ % and 50 % models are slightly (10–20 %) longer than that of $f_{bin} = 0$ % model. This insensitivity of t_{ev} on f_{bin} was noted by McMillan & Hut (1994), and Kroupa (1995b). Kroupa et al. (1999) find that their model with $f_{bin} = 100$ % evolves slightly more slowly than that with $f_{bin} = 60$ % and interpret it due to cooling by disruption of wide binaries. The slightly longer t_{ev} ’s of our models with primordial binaries may be interpreted in the same way, but the reduced number of effective point sources due to binarity may be another possible explanation (the rate of relaxation is proportional to Nm^2 , where m is the stellar mass; when companions are picked out of a pool with a large mass range, the binarity does not

significantly increase the m of an ‘effective point mass’, while it considerably decreases N of the effective point masses).

The number counts with a consideration of the angular resolution of the camera for $f_{bin} = 25\%$ and 50% models are compared to those of the $f_{bin} = 0\%$ model in Figure 5. Here, the mass of a binary system with a semi-major axis smaller than the angular resolution is obtained from the total luminosity of the binary system, and the mass-luminosity relation adopted in Figer et al. (1999) is used for this calculation. While the number counts of the $f_{bin} = 25\%$ model are only slightly smaller than the $f_{bin} = 0\%$ model, those of the $f_{bin} = 50\%$ model are $10\text{--}40\%$ smaller. However, these relatively smaller number counts of models with primordial binaries still agree with observed number counts at an acceptable level. Furthermore, the difference of number counts between the $f_{bin} = 0\%$ and 50% models is larger for the more massive bin, implying that the initial α should be smaller than that of the model tried here (1.75) in order for the $f_{bin} = 50\%$ model to better match the observations. In conclusion, the presence of primordial binaries will not significantly change our findings above on the best-fit initial conditions of the Arches cluster, and our results indicate that the α value found above for the case with no primordial binaries, 1.75, is an upper limit.

5. INITIAL CLUSTER STRUCTURE

5.1. Initial Mass Segregation

The prior sections of the present study and KML assumed, for simplicity, the same initial density profiles for all stellar masses, i.e., no initial mass segregation. This assumption is, however, not based on any observational or theoretical evidence. Interactions between stars during the star formation process determine the degree of initial mass segregation, which is therefore an important piece of information for the theory of cluster formation. However, different models lead to totally different predictions for initial segregation. The model by Podsiadlowski & Price (1992), in which favorable stellar masses are determined by the ratio of the timescales for protostellar collisions and of gas infall onto the protostars, predicts more massive stars at larger radii. On the other hand, segregation of more massive stars in the core is predicted in some models such as the one by Murray & Lin (1996), where encounters between clouplets increase the protostellar masses, and the one by Bonnell et al. (1997), where the deeper potential in the core causes stars there to accrete more circumstellar material. Here we attempt both cases, one with heavy stars initially more prevalent at the core, the other with heavy stars more in the envelope.

The initial density and velocity profiles of model 13 are modified to include the initial mass segregation: model 31 initially has a King profile with $W_0 = 2$ for the lightest stars and $W_0 = 6$ for the heaviest stars (more heavy stars in the envelope) while model 32 has the opposite W_0 values (more heavy stars at the core). The intermediate-mass stars have interpolated W_0 values depending on the logarithm of their masses. We find that models 13, 31, & 32 show very similar

Σ_{20} profiles at 2 Myr. In spite of different initial conditions, the number counts of these three models also exhibit similar evolution after $t = 1$ Myr (see Fig. 6). It appears that the relaxation processes are rapid enough to erase the memory of the initial mass segregation in less than 1 Myr. Thus unless the initial segregation is more severe than models tested here, the best-fit initial conditions found in § 4 are robust against the initial segregation.

5.2. King vs. Plummer Models

KML showed that the global evolution (such as M & R_t) of clusters initially having King profiles of $W_0 = 1\text{--}7$ does not depend on W_0 values. This is because King profiles with different W_0 values mainly differ at the core while the global evolution of the cluster is mostly determined by the properties in the cluster envelope. Here we make two N-body simulations initially having Plummer models to see the effects of initial conditions different from King models. Plummer models have a density profile of

$$\rho \propto (R^2 + R_c^2)^{-5/2}, \quad (5)$$

which has no density drop analogous to tidal cutoff in King models (R_c is the core radius). Thus the density profiles of Plummer models have shallower decrease than King models near R_t , and have to be artificially cut at R_t . The only parameter that determines the profile is the ratio of R_t to R_c , c_p . Here we perform two simulations analogous to model 13 with $c_p = 3$ and $c_p = 6$. The Plummer model with $c_p = 6$ has core density and half-mass radius comparable to those of the King model with $W_0 = 4$. We find that the Plummer models give t_{ev} values only slightly longer than that of the corresponding King model (by less than 20 %), and Σ_{20} and the number counts of the Plummer models are very similar to those of the King model. Therefore, the findings in § 4 may also apply to models with Plummer initial conditions with $c_p = 3\text{--}6$.

6. SUMMARY

Using Aarseth's Nbody6 codes, we have studied the dynamical evolution of CYCs near the GC. First, we confirm the results of KML that clusters with a mass $\lesssim 2 \times 10^4 M_\odot$ evaporate in ~ 10 Myr, but find that the F-P calculations by KML underestimated the lifetimes of CYCs by 5 to 30 % in most cases. This discrepancy is due to the adoption by KML of values of N_u which are too small, and we find that N_u of 250–300 would be appropriate although such a large number would bring the effective mass of the largest mass bin down to a value at which we would lose some of the effects associated with the presence of the most massive stars. Without stellar evolution, the above t_{ev} discrepancy would be more considerable, i.e. the mass loss from stellar evolution starting slightly after $t = 2$ Myr significantly accelerates the evaporation of the clusters. The volume density profiles from F-P calculations are steeper than those from N-body simulations, and especially, the F-P densities outside R_t are significantly underestimated.

By comparing the surface number density profiles and number counts in 2 mass bins at 2 radius bins between N-body simulations and *HST*/NICMOS photometry of the Arches cluster, we find the following best-fit initial conditions: $M = 2 \times 10^4 M_\odot$ and $\alpha = 1.75$. The relation between M and α is constrained by the observed number of stars heavier than $30 M_\odot$, 150. Larger or smaller α values than 1.75 give less satisfactory number count fits to observations. The presence of primordial binaries favors slightly smaller α values than 1.75. The fit of Σ_{20} to observations indicates $R_t \simeq 1$ pc, but R_g is not well constrained. The mean density of the bulge inside the Arches cluster is suggested to be $5-30 \times 10^2 M_\odot \text{pc}^{-3}$. Also, we confirm the finding of KML that for clusters with $\alpha \lesssim 2$, t_{ev} of a cluster with $m_l = 0.1 M_\odot$ is very close to that of a cluster with $m_l = 1 M_\odot$. However, the number count plots seem to more support $m_l = 1 M_\odot$. These findings are in agreement with the arguments by Morris (1993) that the non-standard star formation environment near the GC may lead to an IMF skewed toward relatively massive stars and having an elevated lower mass cutoff.

The global evolution and t_{ev} of CYCs are nearly independent of the initial mass segregation and the choice of initial density profile. Clusters with initial mass segregation and reverse segregation (more heavy stars in the outer region) show very similar evolution except in the very early phase (< 0.5 Myr). Plummer initial models with $c_p = 3$ and 6 exhibit indistinguishable evolution from a King initial model. Therefore, our findings regarding the initial conditions of the Arches cluster appear to be insensitive to the initial mass distribution.

As discussed in KML, the effect of the gas left over from cluster formation may be important to the early dynamical evolution of CYCs because the remnant gas is thought to be blown away from the cluster in the early phases by strong stellar winds or supernova explosions, and such abrupt disappearance may significantly change the potential of the cluster in a short amount of time. Consequently, the role of the remnant gas in early cluster evolution will be the subject of a future study using N-body simulations.

S.S.K. is deeply grateful to Sverre Aarseth for generously providing us with his Nbody6 codes and for his kind help with the codes. S.S.K. also appreciates Pavel Kroupa, Kap Soo Oh, Simon Portegies Zwart, and Koji Takahashi for helpful discussions. We thank the referee for valuable suggestions and comments. This work was partially supported by a NASA grant to UCLA, and H.M.L. acknowledges the support from the KOSEF through grant 1999-2-113-001-5.

REFERENCES

Aarseth, S. J. 1999, PASP, 111, 1333
Becklin, E. E., & Neugebauer, G. 1968, ApJ, 151, 145
Bonnell, I. A., Bate, M. R., Clarke, C. J., & Pringle, J. E. 1997, MNRAS, 285, 201
Durisen, R. H., & Sterzik, M. F. 1994, A&A, 286, 84

Figuer, D. F., Kim, S. S., Morris, M., Serabyn, E., Rich, R. M., & McLean, I. S. 1999, *ApJ*, 525, 750

Kim, S. S., Morris, M. & Lee, H. M. 1999, *ApJ*, 525, 228 (KML)

Kroupa, P. 1995a, *MNRAS*, 277, 1507

Kroupa, P. 1995b, *MNRAS*, 277, 1522

Kroupa, P., Petr, M. G., & McCaughrean, M. J. 1999, *New Astronomy*, 4, 495

Lindqvist, M., Habing, H. J., & Winnberg, A. 1992, *A&A*, 259, 118

McMillan, S., & Hut, P. 1994, *ApJ*, 427, 793

Meynet, G., Maeder, A., Shaller, G., Shaerer, D., & Charbonnel, C. 1994, *A&AS*, 103, 97

Morris, M. 1993, *ApJ*, 408, 496

Murray, S. D., & Lin, D. N. C. 1996, *ApJ*, 467, 728

Podsiadlowski, P., & Price, N. M. 1992, *Nature*, 359, 305

Portegies Zwart, S. F., Makino, J., McMillan, S. L. W., & Hut, P. 1999, *A&A*, 348, 117

Portegies Zwart, S. F., et al. 2000, in preparation

Scalo, J. M. 1986, *Fundamentals of Cosmic Phy.*, 11, 1

Takahashi, K., & Portegies Zwart, S. F. 1998, *ApJ*, 503, L49

Table 1. Comparison of t_{ev} between N-body & F-P Calculations

Model	KML	M	α	m_l	N	R_g	t_{ev} (Myr)		$\Delta't_{ev}$ (%)
		(M_\odot)		(M_\odot)		(pc)	N-body	F-P	
1	142	2×10^4	2.35	1.0	6270	30	5.5	4.0	27
3	115	2×10^4	1.50	0.1	5164	30	2.8	2.2	21
5	141	5×10^3	2.35	1.0	1567	30	2.4	2.2	8
8	113	2×10^4	1.50	1.0	1633	30	2.7	2.3	15
13	...	2×10^4	1.75	1.0	2605	30	2.8	2.4	14
15	...	2×10^4	1.75	0.1	12706	30	3.0	2.6	13
23	101	2×10^4	2.00	1.0	6270	30	3.6	2.7	25
43	...	2×10^4	1.75	1.0	2605	10	2.2	0.9	59
44	...	2×10^4	1.75	1.0	2605	100	4.5	3.8	16

Note. — F-P values are from KML except for models with $\alpha = 1.75$, which were additionally calculated for the present study. The coefficient for the speed of star removal, α_{esc} , of 2 is adopted for all F-P simulations here. Column KML is for the model numbers from the paper KML. $\Delta't_{ev}$ is the fractional difference, $|FP-Nbody|/Nbody$.

Table 2. Number Counts from the Observation of the Arches Cluster

Radius Bin	Mass Bin	
	$8 \leq m/M_\odot \leq 20$	$20 \leq m/M_\odot$
$0.4 \leq r/\text{pc} \leq 0.8$	64	46
$0.2 \leq r/\text{pc} \leq 0.4$	66	56

Table 3. N-body Simulations for the Arches' Initial Conditions

Model	M (M_{\odot})	m_l (M_{\odot})	R_g (pc)	t_{ev} (Myr)
13	2.0×10^4	1.75	1.0	30
14	2.0×10^4	1.75	1.0	50
15	2.0×10^4	1.75	0.1	30
19	2.0×10^4	1.75	1.0	20
21	1.6×10^4	1.50	1.0	30
22	2.8×10^4	2.00	1.0	30

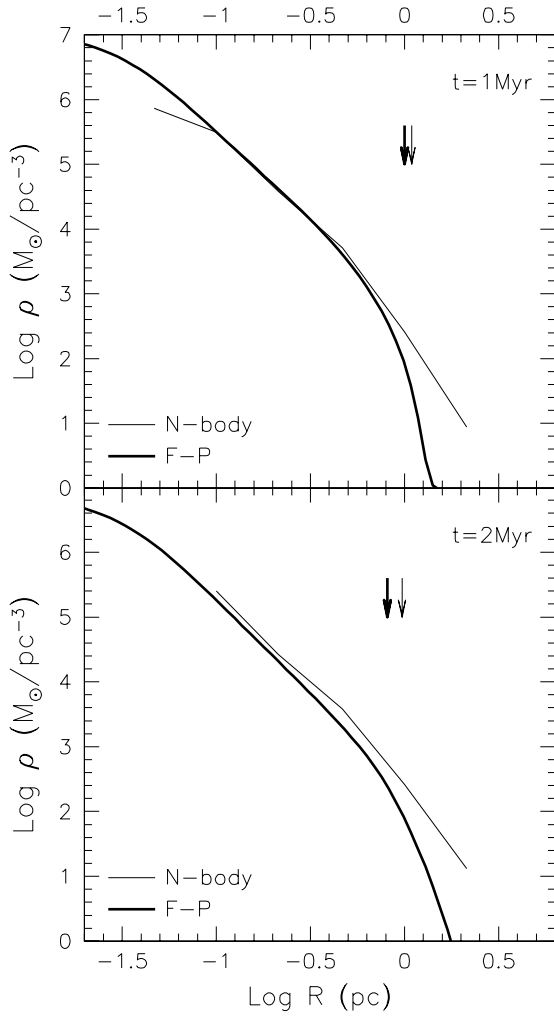


Fig. 1.— Volume density profiles of N-body (*thin lines*) and F-P (*thick lines*) calculations for model 13 at $t = 1$ Myr (*upper panel*) and 2 Myr (*lower panel*). The locations of tidal radii are marked with arrows. $N_u = 250$ and $N_{\text{bin}} = 10$ were used for the F-P calculation.

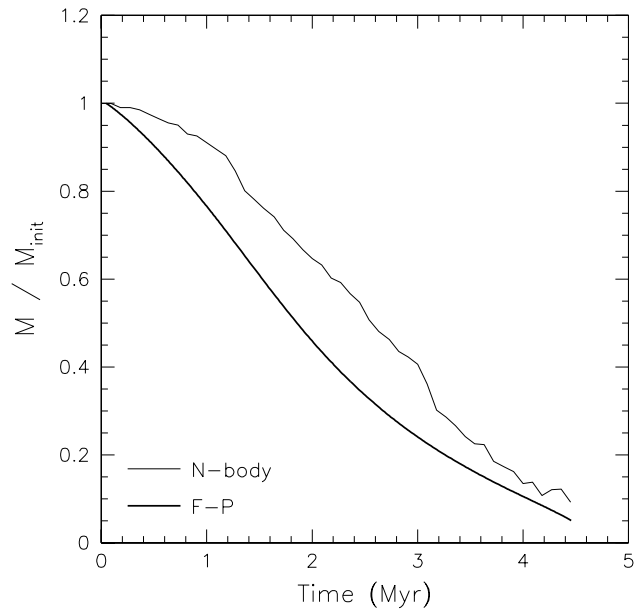


Fig. 2.— Evolution of cluster mass inside the tidal radius, M , of N-body (thin lines) and F-P (thick lines) calculations for model 13. M 's are normalized to their initial values. Stellar evolution is not included in these calculations, and $N_u = 250$ and $N_{\text{bin}} = 10$ were used for the F-P calculation.

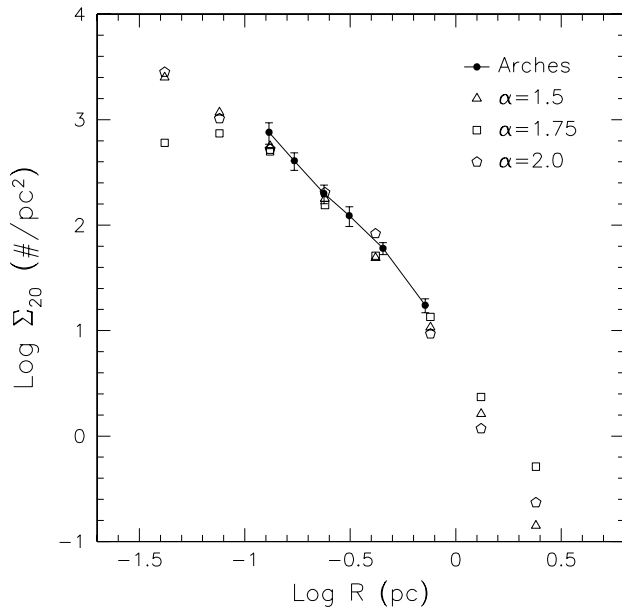


Fig. 3.— Surface number density profiles of stars heavier than $20 M_{\odot}$, Σ_{20} , from our N-body models 21 ($\alpha = 1.5$; *triangles*), 13 ($\alpha = 1.75$; *squares*), & 22 ($\alpha = 2.0$; *pentagons*), and NICMOS observations of the Arches by Figer et al. (1999; *solid circles connected with a line*). N-body results shown are the ones at $t = 2$ Myr for models 13 & 22, and $t = 1$ Myr for model 21 (model 21 shows a worse fit for the core region at $t = 2$ Myr). The tidal radii of N-body models 21, 13, & 22 at the epoch shown here are 1.0 pc, 1.0 pc, & 1.2 pc, respectively. The observations are limited by crowding at the core and by background confusion near and outside the tidal radius. $1-\sigma$ Poisson errors for observations are indicated by vertical bars.

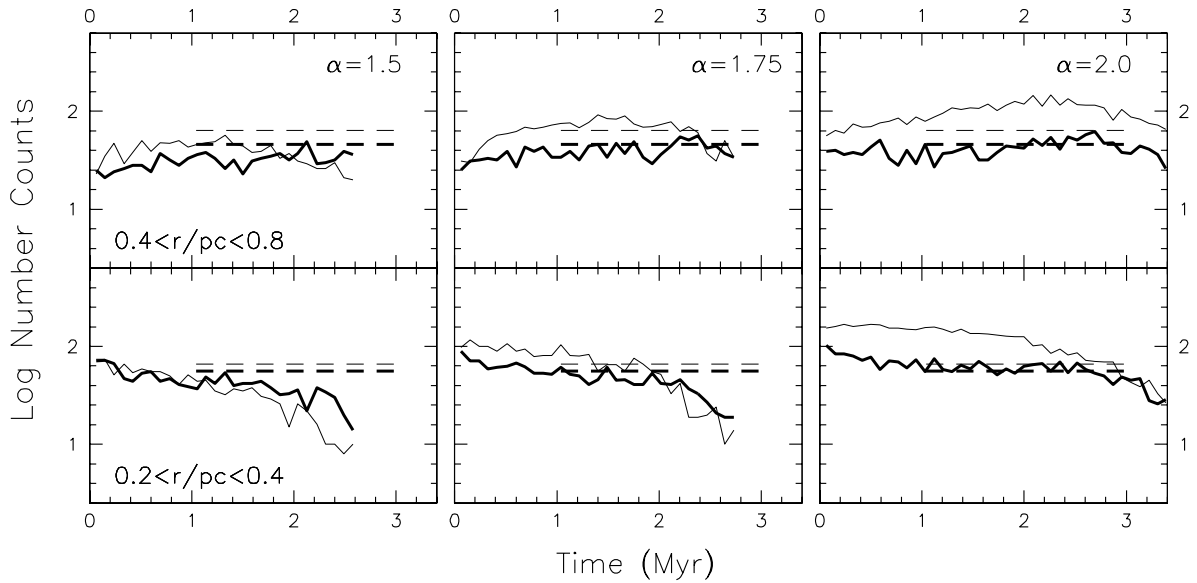


Fig. 4.— Evolution of number counts of stars with $8 \leq m/M_{\odot} \leq 20$ (thin lines) and stars with $20 \leq m/M_{\odot}$ (thick lines) in the $0.2 < r/\text{pc} < 0.4$ region (lower panels) and the $0.4 < r/\text{pc} < 0.8$ region (upper panels), from our N-body models 21 ($\alpha = 1.5$; solid lines in left panels), 13 ($\alpha = 1.75$; solid lines in middle panels), & 22 ($\alpha = 2.0$; solid lines in right panels), and NICMOS observations of the Arches by Figer et al. (1999; dashed lines). The dashed lines cover the estimated age of the Arches cluster, 2 ± 1 Myr.

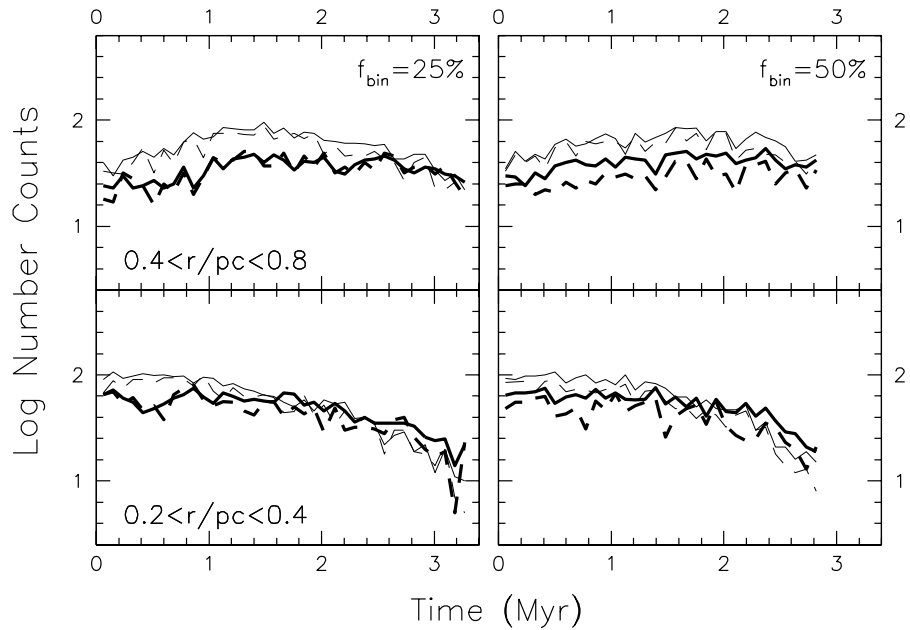


Fig. 5.— Evolution of number counts of stars with $8 \leq m/M_{\odot} \leq 20$ (thin lines) and stars with $20 \leq m/M_{\odot}$ (thick lines) in the $0.2 < r/\text{pc} < 0.4$ region (lower panels) and the $0.4 < r/\text{pc} < 0.8$ region (upper panels), from our N-body model 13 with $f_{\text{bin}} = 25\%$ (dashed lines in left panels) and model 13 with $f_{\text{bin}} = 50\%$ (dashed lines in right panels). The angular resolution of the *HST*/NICMOS camera 2, $\sim 0.075''$, is considered in counting apparent numbers and estimating apparent masses (see text for details). Model 13 with $f_{\text{bin}} = 0\%$ (solid lines in both panels) is also plotted for comparison.

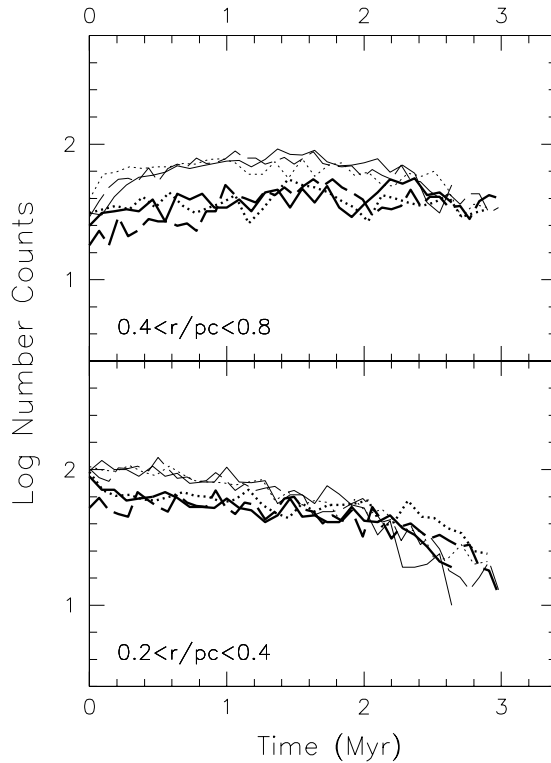


Fig. 6.— Evolution of number counts of stars with $8 \leq m/M_{\odot} \leq 20$ (thin lines) & stars with $20 \leq m/M_{\odot} \leq 20$ (thick lines) in the $0.2 < r/\text{pc} < 0.4$ region (lower panel) and the $0.4 < r/\text{pc} < 0.8$ region (upper panel), from our N-body models 13 (no initial segregation; solid lines), 31 (initially more heavy stars in the envelope; dashed lines), & 32 (initially more heavy stars in the core; dotted lines).